J. Fluid Mech. (1976), *vol.* 73, *part* 2, *pp.* 305–332
Printed in Great Britain

The initial region of subsonic coaxial jets

By N. W. M. KO AND A. S. H. KWAN
Department of Mechanical Engineering, University of Hong Kong

(Received 11 July 1975)

This paper describes part of a detailed study of the initial region of coaxial jets of three different mean-velocity ratios. Similarity of the mean-velocity and turbulent-intensity profiles within the two mixing regions inside the initial merging zone, and within the mixing region inside the fully-merged zone, has been observed. Similarity with single-jet results has been obtained. Overall pressure measurements and hot-wire and microphone spectra inside coaxial jets yield two pronounced peaks, suggesting the existence of two types of vortices at different frequencies. The higher-frequency or primary vortices are found to be generated in the primary or inner mixing region, and the lower-frequency or secondary ones in the secondary or outer mixing region. It seems that the former are generated further upstream than the latter. Both types of vortices are found in the initial merging zone. However, their growth or decay and their dominance depend on the mean-velocity ratio. Low mean-velocity ratios indicate the dominance of the high-frequency vortices. At high mean-velocity ratios, the low-frequency vortices are dominant. The Strouhal number of the vortices plays an important part in their growth and decay. The complicated flow structure of coaxial jets can be very simply related to, and described by, the much simpler structure of single jets.

1. Introduction

The initial region of homogeneous coaxial jets discharging into stationary air has been investigated by a number of workers. One can easily cite the work of Forstall & Shapiro (1950), Chigier & Beer (1964), Gelb & Martin (1966) and Williams, Ali & Anderson (1969). The above investigations covered coaxial jets of different exit velocity, mean-velocity ratio, nozzle diameter and area ratio. However, they attended mainly to the mean flow characteristics, such as the mean profiles of the coaxial jets and their mean-velocity distributions.

In these mean-velocity results, elongation of the primary or inner potential core length was observed. Further, the results of Williams *et al.* (1969) showed similarity of the mean-velocity profiles at a distance greater than six primary diameters downstream. No similarity was obtained for the profiles within the first six diameters.

The purpose of the present investigation was to obtain information about the flow characteristics within the initial region of coaxial jets. The coaxial jets were run at three different mean-velocity ratios, secondary to primary, which were less than unity. A preliminary work of the authors has been published elsewhere: Ko & Kwan (1974). The investigation was divided into two parts. This paper presents the first part of the investigation, which concerns turbulence and

pressure measurements. The second part concerns correlation measurements of the whole initial region.

Within the initial region, seven primary diameters from the nozzle exits, both the mean and fluctuating components of velocity inside the two potential cones and the two corresponding mixing or shear regions were obtained and are presented. From these measurements, the initial region can be divided into different zones: the initial merging, intermediate and fully-merged zones.

Pressure fluctuations inside the coaxial jets were also measured in detail. Comparison with the results on velocity fluctuations will be attempted, so that the location of vortices generated within the two mixing regions is isolated, and its dominance considered.

Basic understanding of the noise mechanism within the mixing region of single jets has been increased in the last few years. Coherent structure or vortices in the shear region have been reported by Mollo-Christensen, Kolpin & Martuccelli (1964), Bradshaw, Ferriss & Johnson (1964), Crow & Champagne (1971), Lau, Fisher & Fuchs (1972), Laufer (1974) and Chan (1974). Thus, it was also the purpose of the present work to investigate the noise mechanism of the coaxial jets, to find out whether there is any similarity between the mechanisms of single and coaxial jets.

2. Apparatus

The experiments were carried out within coaxial air jets that mix externally. The central nozzle, which generated the primary or inner jet, has a diameter of 2·10 cm. The area contraction ratio of this nozzle was 13 : 1. The secondary or outer jet was produced by an annular nozzle which has an outer diameter of 4 cm. The corresponding area contraction ratio was 8 : 1. Deducting the area due to the wall thickness at the primary nozzle exit, the area ratio β of the secondary to primary nozzles was 2·67.

The wall thickness at the primary nozzle exit was kept to a minimum. The reason was that a fairly discrete tone was generated owing to the discontinuity in the nozzle profile at the exit and the difference in the mean velocity at the primary and secondary jets. This fairly discrete tone was also observed by Eldred *et al.* (1971). Even with the feasible minimum thickness of 0·078 cm, the tone was observed at above 10 kHz. Since it was beyond the frequency range of main interest, the effect was neglected.

Both nozzles were supplied with dry, oil-free, high-pressure air from an air reservoir. The nozzles have Burgess-type silencers as their settling chambers, and the noise from the control gate valves was mostly absorbed by two resonator-type silencers before it arrived at the nozzle exits. Thus, the inherited overall background pressure level of both nozzles was 100 dB. Furthermore, the turbulence intensity was 0·4 and 0·7 % of the mean exit velocity for the inner and outer nozzle, respectively.

The hot-wire anemometer used was a constant-temperature type with linearized output (Davies & Davis 1966). The wire had a diameter of 5×10^{-6} m and a length of 2 mm. The operating resistance was 15 Ω.

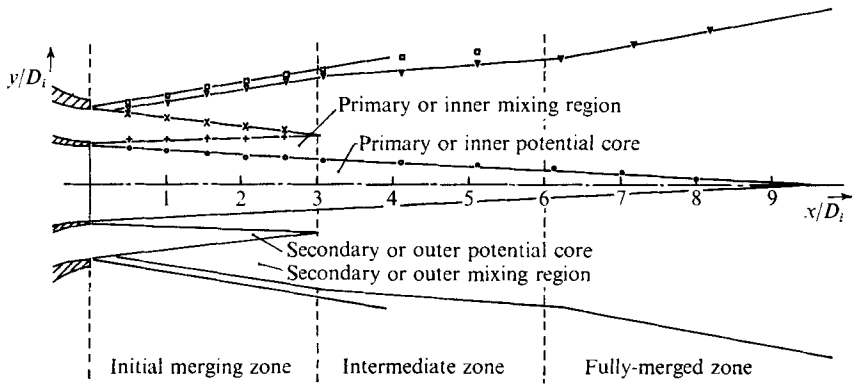

FIGURE 1. Profile of initial region coaxial jet. $\lambda = 0{\cdot}7$. $\overline{U}$: ○, $0{\cdot}995\,\overline{U}_i$; +, $0{\cdot}05\,(\overline{U}_i - \overline{U}_0)$; ×, $0{\cdot}995\,\overline{U}_0$; ▽, $0{\cdot}05\,\overline{U}_i$; □, $0{\cdot}05\,\overline{U}_0$.

The microphone used for pressure measurements was the Brüel & Kjaer $\frac{1}{8}$ in. diameter condenser type. The corresponding nose cone was adopted for the pressure measurements inside the jets. The suitability of using a condenser microphone for measuring fluctuating pressure in a turbulent jet has been discussed by Fuchs (1972). Because the size of the condenser microphone was comparable with the sizes of the coaxial jets, performance of the microphone was checked against a microphone with a hypodermic tube, as suggested by Nakamura *et al.* (1969). No appreciable difference was found.

The 6% constant-percentage bandwidth spectra of both the velocity and pressure fluctuations were obtained with a Brüel & Kjaer frequency analyser, Type 2107, together with a Brüel & Kjaer level recorder, Type 2305.

The domain of investigation will mostly be confined within the first seven diameters of the primary jet D_i downstream from the nozzle exits. The mean exit velocity of the primary jet $\overline{U}_i$ was $60\,\mathrm{m\,s^{-1}}$. The mean-velocity ratios λ of the secondary to primary jet $\overline{U}_0/\overline{U}_i$ were 0·3, 0·5 and 0·7.

3. Mean velocity

The mean-velocity profiles of coaxial jets have been obtained by Forstall & Shapiro (1950), Chigier & Beer (1964), Williams *et al.* (1969) and others. Combined with the results of this investigation, different zones of coaxial jets can be distinguished (figure 1). Since the mean exit velocity of the secondary or outer jet is lower than that of the primary or inner jet, i.e. the mean-velocity ratio λ is less than unity, the primary potential core is relatively much longer than that of a simple jet. The zone which is nearest the nozzle exits and ends roughly at the place where the secondary or outer potential core disappears is called the initial merging zone. The termination of this zone, however, depends on the mean-velocity ratio λ. Thus, it is within this zone that two potential cores, both primary and secondary, are found. Also, in this zone the outer boundary of the secondary mixing region, at $\overline{U}/\overline{U}_0 = 0{\cdot}05$, has a linear relationship with axial distance (figure 1). Immediately downstream from the initial merging zone is the

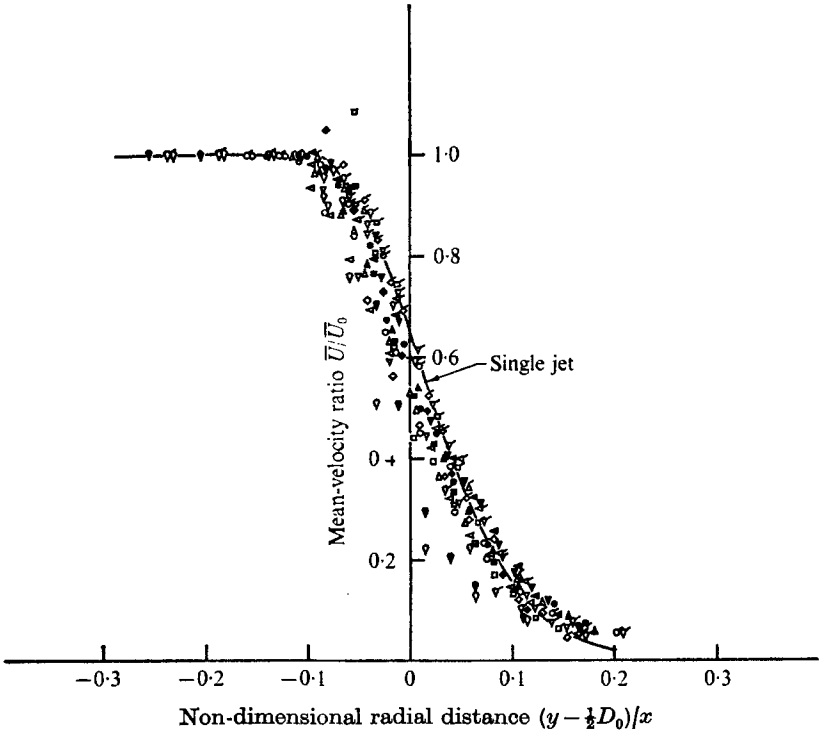

FIGURE 2. Non-dimensional plot of mean velocity ratio in the secondary mixing region. $\lambda = 0{\cdot}3$. x/D_i: ▵, 0·5; ▽, 1; ○, 1·5; △, 2; ◁, 2·5; ▽, 3; ◇, 4; □, 5; ▷, 6; ⬠, 7. $\lambda = 0{\cdot}5$. x/D_i: ▲, 0·5; ▼, 1; ●, 1·5; ▲, 2; ◀, 2·5; ▼, 3; ◆, 4; ■, 5; ▶, 6; ⬟, 7. $\lambda = 0{\cdot}7$. x/D_i: ▵, 0·5; ▽, 1; ○, 1·5; △, 2; ◁, 2·5; ▽, 3; ◇, 4; □, 5; ▷, 6; ⬠, 7.

intermediate zone, where the primary potential cone still exists. It is within this zone that mixing of the flows from the two upstream mixing regions occurs. The extent of this intermediate zone is about two to three primary diameters. The fully-merged zone is the one downstream from the intermediate zone. The initial merging zone, the outer boundary of the combined or merged jet, at $\overline{U}/\overline{U}_i = 0{\cdot}05$, has a linear relationship with axial distance. The extent of the primary potential core depends on the mean-velocity ratio. This is a brief description of the three zones in the initial region of coaxial jets. Better distinction of the different zones will become clearer when the similarity of the mean-velocity and turbulence-intensity profiles is considered.

Similarity of the local mean-velocity profiles of the outer mixing region is shown in figure 2. The non-dimensional velocity ratio $\overline{U}/\overline{U}_0$ is plotted against the non-dimensional radial distance $\eta_0 = (y-\frac{1}{2}D_0)/x$. Both the mean exit velocity $\overline{U}_0$ and the outer diameter D_0 at the exit of the secondary nozzle are used. From figure 2 good similarity is found for the results for $\lambda = 0{\cdot}5$ and 0·7. Though there is slight deviation in the results for $\lambda = 0{\cdot}3$, fairly good similarity is still obtained. With each velocity ratio λ, similarity is observed between the axial positions $1{\cdot}5 \leqslant x/D_i \leqslant 4$. For $x/D_i \leqslant 1{\cdot}5$, the loss of similarity in the local mean-velocity profile is due to different characteristics within the region very near the exit. This agrees with the single-jet result of Ko & Davies (1971) that similarity could not

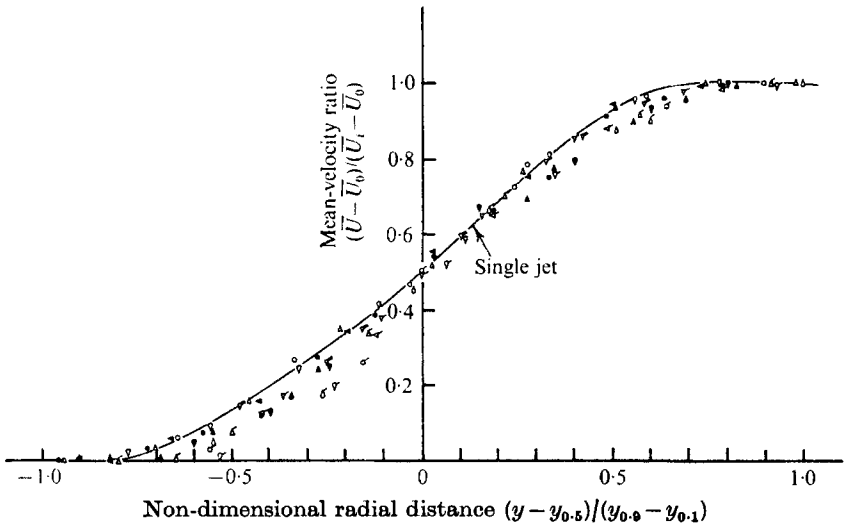

FIGURE 3. Non-dimensional plot of mean velocity ratio in the primary mixing region. Symbols same as figure 2.

be obtained within the first diameter downstream from the nozzle exit. For $x/D_i \geqslant 4$, however, the loss of similarity suggests a different zone, that is, the intermediate zone. The similarity curve of the local mean-velocity ratio of single jets obtained by Davies, Fisher & Barratt (1963), Mollo-Christensen *et al.* (1964), Bradshaw *et al.* (1964) and Ko & Davies (1971) is also shown in figure 2. The good agreement between the coaxial-jet and the single-jet results suggests that the outer mixing region behaves exactly like that of a single jet.

Good similarity of the local mean velocity $(\overline{U}-\overline{U}_0)/(\overline{U}_i-\overline{U}_0)$ in the inner mixing region with non-dimensional radial distance $\eta_i' = (y-\frac{1}{2}D_i)/x$ is found for $\lambda = 0{\cdot}3$ and 0·5 (not shown). A slight discrepancy is observed for $\lambda = 0{\cdot}7$. The probable reason for this discrepancy is the small difference in the exit velocity between the inner and outer jets. Because of this, another set of results for the same λ (0·7), but at a higher exit velocity, was obtained. These give better similarity. Although similarity is obtained within $0{\cdot}5 \leqslant x/D_i \leqslant 3$, the curve is much narrower than that of single jet. The reason is mainly that the primary jet behaves like a jet discharging into a uniform moving stream (Gelb & Martin 1966; Abramovich 1963). In this respect, the width of the inner mixing region would then be smaller than that of single jet.

However, by adopting the non-dimensional radial distance of

$$\eta_i = (y-y_{0\cdot5})/(y_{0\cdot9}-y_{0\cdot1}),$$

instead of η_i', better agreement with the coaxial-jet results of Abramovich (1963) and the single-jet results is found (figure 3). The definition of $y_{0\cdot9}$, $y_{0\cdot5}$ and $y_{0\cdot1}$ is the radial position where the local mean velocity is equal to 0·9, 0·5 and 0·1 of $(\overline{U}_i-\overline{U}_0)$ respectively. Comparison of the axial distances where similarity is found shows that both the inner and outer mixing region give the same distance. This suggests that the same distance is more or less required for the development and

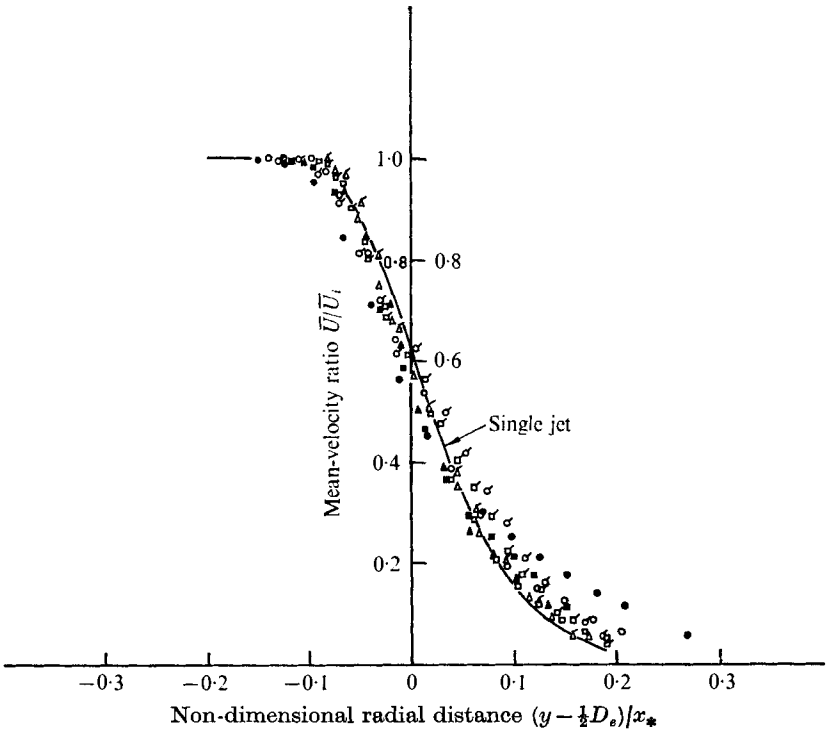

FIGURE 4. Non-dimensional plot of mean-velocity ratio in the intermediate and fully-merged zones. $\lambda = 0{\cdot}3$. x/D_i: ○, 6; □, 7; △, 8. $\lambda = 0{\cdot}5$. x/D_i: ●, 6; ■, 7; ▲, 8. $\lambda = 0{\cdot}7$. x/D_i: ◔, 6; ◧, 7; ◭, 8.

maintenance of the flow before changes occur. Further comparison shows that in the inner mixing region similarity starts one primary diameter further upstream than in the outer mixing region. This means that the former starts at $x/D_i = 0{\cdot}5$, the latter at $x/D_i = 1{\cdot}5$. This axial distance of $x/D_i = 1{\cdot}5$ for the outer mixing region agrees with the single-jet results of Ko & Davies (1971).

The discrepancy of the inner mixing region may be due to the characteristics of the inner jet, which is discharging into a uniform stream. Again, it may be due to the presence of the lip of the inner nozzle. The wake formed behind the lip may act like a tripping wire, and result in earlier transition to the turbulent regime (Crow & Champagne 1971). This would then be responsible for the earlier occurrence of similarity.

From the axial positions $x/D_i \geqslant 4$ no similarity is found for the local mean velocity profile. This is within the intermediate zone, where the secondary potential cone has disappeared and the mixing of the two mixing regions occurs. In a way, this behaves like the transition region of the single jet $5 \leqslant x/D_i \leqslant 8$, where similarity is not found and mixing occurs owing to the disappearance of the cone.

In the fully-merged zone $x/D_i \geqslant 6$, similarity of the velocity profile is again achieved (figure 4). The same phenomenon was found by Williams *et al.* (1969) and Eldred *et al.* (1971). The similarity of the local mean velocity $\overline{U}/\overline{U}_i$ to the

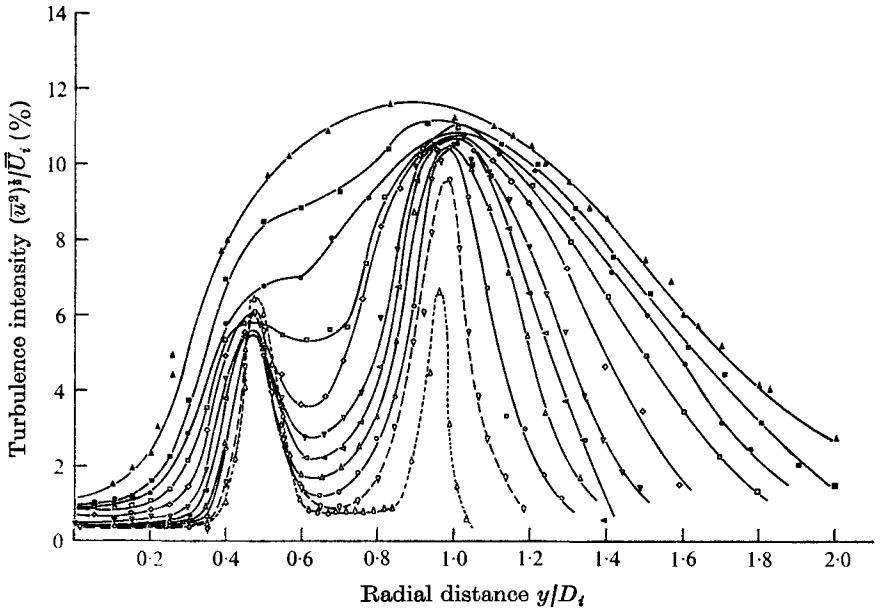

FIGURE 5. Radial distribution of turbulence intensity level. $\lambda = 0{\cdot}7$. x/D_i: ◊, 0·5; ▽, 1; ○, 1·5; △, 2; ◁, 2·5; ▽, 3; ◇, 4; □, 5; ●, 6; ■, 7; ▲, 8.

non-dimensional radial distance $\eta_e = (y - D_e/2)/x_e$ is derived from the idea of Eldred *et al.* (1971) that this zone can be represented by an equivalent jet of identical thrust having a diameter D_e and an equivalent exit velocity $\overline{U}_e$. The equivalent diameter can be represented by $(1+\lambda^2\beta)^{\frac{1}{2}} D_i$, where λ is the exit mean velocity ratio and β the exit area ratio, both secondary and primary. In this case, the equivalent $\overline{U}_e$ is equal to $\overline{U}_i$.

This equivalent jet has a different axial position for its virtual origin. As can be visualized, this virtual origin is a function of the mean velocity ratio λ. Over the range of λ considered in this investigation, the smaller the λ, the bigger the shift of the virtual origin Δx downstream. Thus, the axial distance adopted for the equivalent jet would then be $x_e = x - \Delta x$.

4. Turbulence intensity

A typical axial distribution of the turbulence intensity profiles of coaxial jets is shown in figure 5. The mean-velocity ratio λ is equal to 0·7. Basically, there are two low-intensity regions, which correspond to the locations of the two potential cones. The two-high intensity regions correspond to the two mixing regions. From $x/D_i = 6$, only one mixing region is found.

A closer look at the primary potential cone indicates that the turbulence intensity level $(\overline{u^2})^{\frac{1}{2}}/\overline{U}_i$ at the axis is only about 1 % even at the axial position $x/D_i = 8$. Taking into account the different values of λ, the highest intensity at $x/D_i = 8$ is found at $\lambda = 0{\cdot}3$, only about 3 %. It is lower than the corresponding level of the single jet (Ko & Davies 1971).

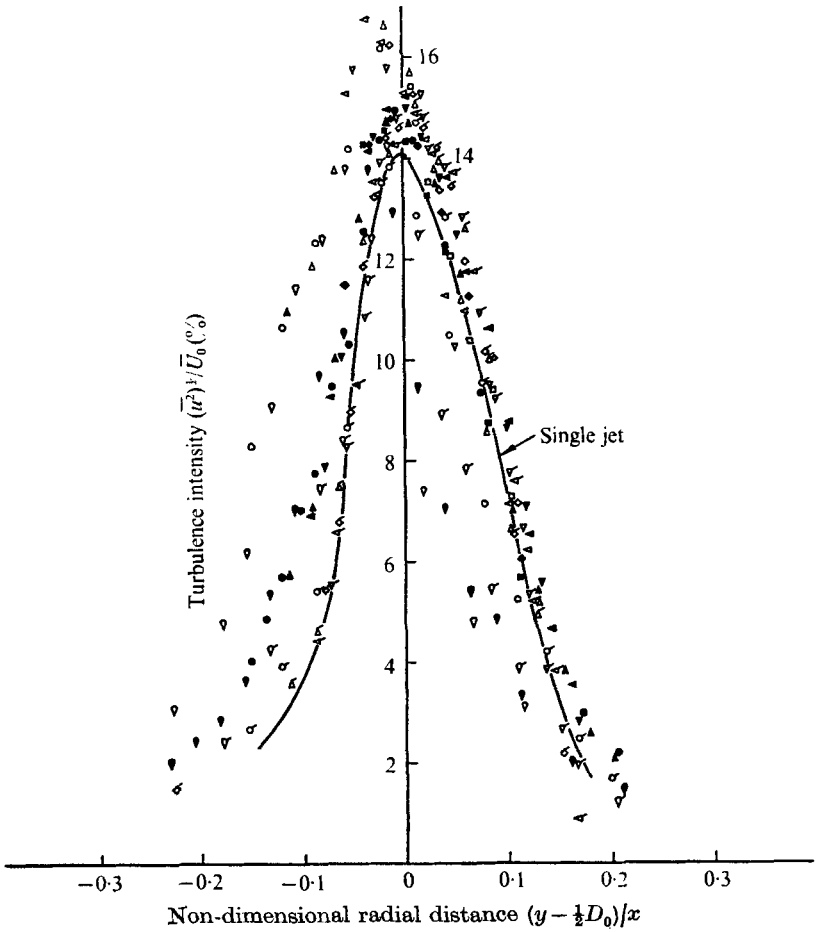

FIGURE 6. Non-dimensional plot of turbulence intensity level in the secondary mixing region. Symbols same as figure 2.

Similarity of the turbulence intensity $(\overline{u^2})^{\frac{1}{2}}/\overline{U}_0$ to the non-dimensional radial distance of the outer mixing region within the initial merging zone is shown in figure 6. The same η_0 is used for the non-dimensional radial distance. Although similarity within the axial distance $1{\cdot}5 \leqslant x/D_i \leqslant 4$ for each velocity ratio λ is found, there is slight variation for different λ. Compared with the single-jet results, the lower the λ, the more deviation there is from the single jet. The deviation is progressively reduced as the λ increases. This seems logical, because one would suspect that with the increase in λ the coaxial jets behave more like a single jet.

Deviation of the similarity curve is only true for $\eta_0 \leqslant 0$. This means that no difference exists between the single jet and the coaxial jets for $\eta_0 \geqslant 0$. This phenomenon is very interesting. It may suggest that the outer part of the secondary mixing region is fairly insensitive to any changes in the exit velocity of the outer nozzle. The sensitivity of the inner part of the mixing region, where the vortices are generated and convected downstream (as found by Ko & Davies

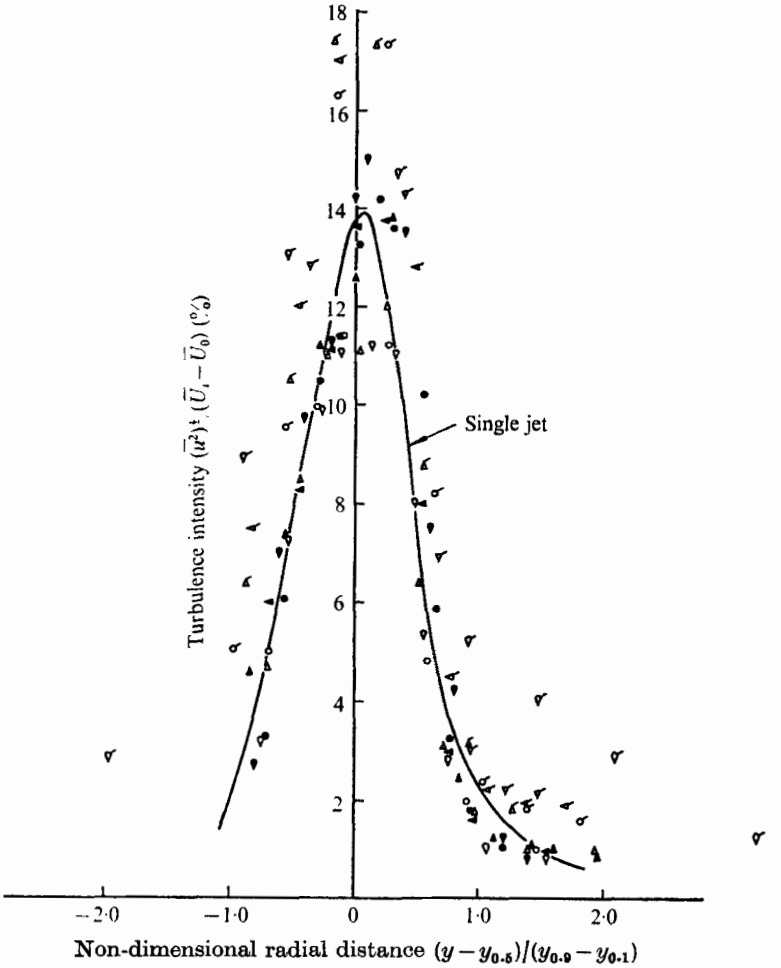

FIGURE 7. Non-dimensional plot of turbulence intensity level in the primary mixing region. Symbols same as figure 2.

1971; Lau *et al.* 1972; Ko & Davies 1975), may be due to a difference in the generation and convection of vortices at different exit velocities $\overline{U}_0$ of the outer nozzle. Furthermore, this difference in exit velocity $\overline{U}_0$ may also result in a difference in shear and characteristics of the vortices generated. Further discussion of this aspect will be attempted in §§ 6 and 7, on spectral measurements.

Also from figure 6, the maximum turbulence intensity, about 15–16 %, of the coaxial jets is not situated at $\eta_0 = 0$, as in the single-jet results. The smaller the λ, the greater the shift of the maximum turbulence intensity towards the axis of the jets. This shift indicates that the outer jet is deflected towards the axis. With lower λ (i.e. lower outer jet exit velocity), the inner jet is more dominant. The higher entrainment by the inner jet would then draw the outer jet more towards the axis. This may also be the cause of the poor similarity at $\eta_0 \leqslant 0$.

Within the initial merging zone, the turbulence intensity $(\overline{u^2})^{\frac{1}{2}}/(\overline{U}_i - \overline{U}_0)$ of the inner mixing region is shown in figure 7. The same non-dimensional radial

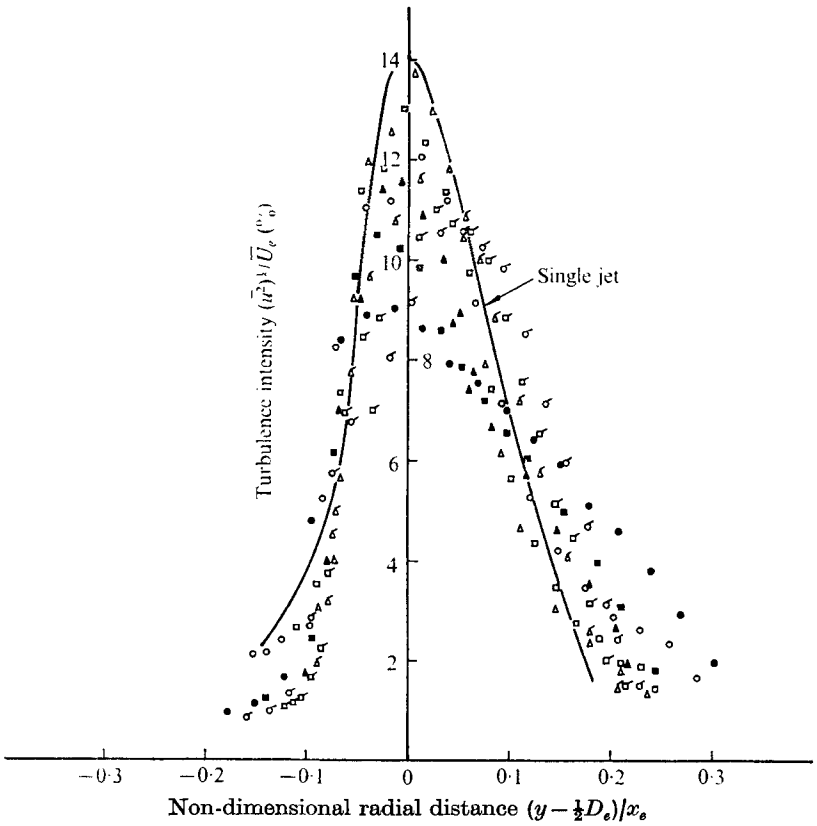

FIGURE 8. Non-dimensional plot of turbulence intensity level in the intermediate and fully-merged zones. Symbols same as figure 4.

distance $\eta_i = (y-y_{0\cdot5})/(y_{0\cdot9}-y_{0\cdot1})$ is used. On the whole, the turbulence-intensity curves have opposite trends from those in the outer mixing region (figure 7). This means that the maximum turbulence intensity, about 14–17 % of $(\overline{U}_i-\overline{U}_0)$, occurs at a slightly positive value of η_i. Similarity of the turbulence profiles is also shown in figure 7 between the axial positions $1 \leqslant x/D_i \leqslant 3$. However, that at $\lambda = 0{\cdot}7$ tends not to be as good as the other two.

In the fully-merged zone, similarity of the turbulence intensity $(\overline{u^2})^{\frac{1}{2}}/\overline{U}_i$ is found with $\eta_e = (y-D_e/2)/x_e$ (figure 8) for the axial positions $x/D_i \geqslant 7$. With the results of the initial merging zone, poorer similarity is obtained. For $x/D_i \leqslant 7$, within the intermediate zone, very distinct deviation from the similarity curve is found. Also from figure 8, there is not much difference between the results in the inner part of the mixing region of single and coaxial jets. This is similar to the results in the outer part of the secondary mixing region shown in figure 6. This again suggests that any change in λ does not change the inner portion of the mixing region much, but rather changes the outer portion of the region. This change in the fully-merged zone seems logical, because the mixing of the secondary and primary mixing regions occurs in the intermediate zone.

It has been found in §§ 3 and 4 that there is similarity in the local mean-velocity

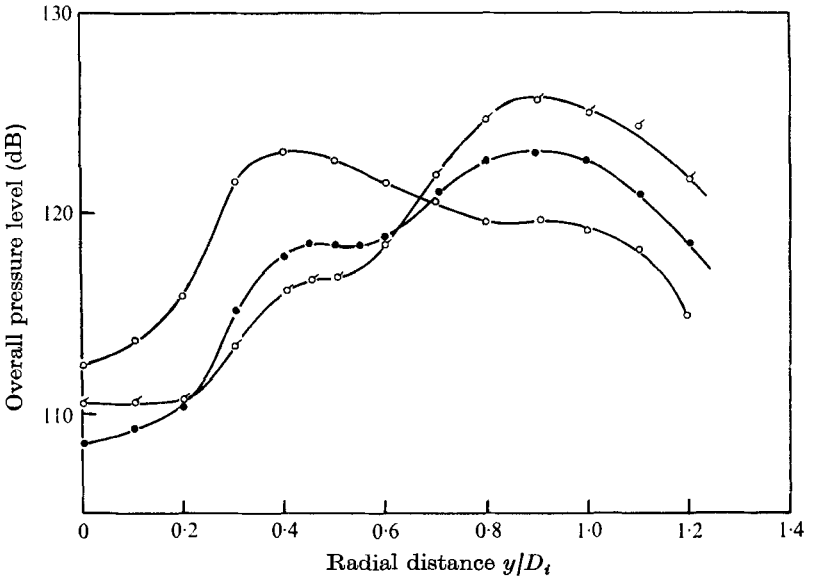

FIGURE 9. Radial distribution of overall pressure level in initial merging zone. $x/D_i = 2$. λ: ○, 0·3; ●, 0·5; ♂, 0·7.

ratio and the turbulence intensity in the primary and secondary mixing regions within the initial merging zone and in the fully-merged zone. No similarity could be found in the intermediate zone. Further, it is found that the secondary mixing region in the fully-merged zone behaves like a single jet. By contrast, the primary mixing region behaves like a jet discharging into a moving stream.

5. Overall pressure levels

The overall pressure levels obtained inside the three zones are shown in figures 9–11. In the initial merging zone $x/D_i = 2$ (figure 9), two peaks are observed in the radial distribution of the overall pressure levels. These are found in all the results for the three coaxial jets.

The peaks nearer to the coaxial-jet axis, called primary peaks, are inside the primary or inner mixing region (figure 1). The exact position, which will be discussed in more detail later, is not found at the location of maximum intensity, but nearer the boundary of the primary potential cone. This phenomenon agrees fairly well with the location of the vortices in the single jet, as observed by Chan (1974) and Ko & Davies (1975).

From figure 9 the maximum pressure level of the primary peak increases with the decrease in the mean velocity ratio λ. It increases from about 116 dB at $\lambda = 0{\cdot}7$ to 123 dB at $\lambda = 0{\cdot}3$. With the disappearance of the secondary jet (i.e. for a single jet), the level increases further to 131 dB. This shows that the overall pressure level of the primary peak decreases with the introduction of and the increase in the exit velocity of the secondary jet. This shows the same trend as the far-field results of Williams *et al.* (1969). At roughly the same area ratio as the

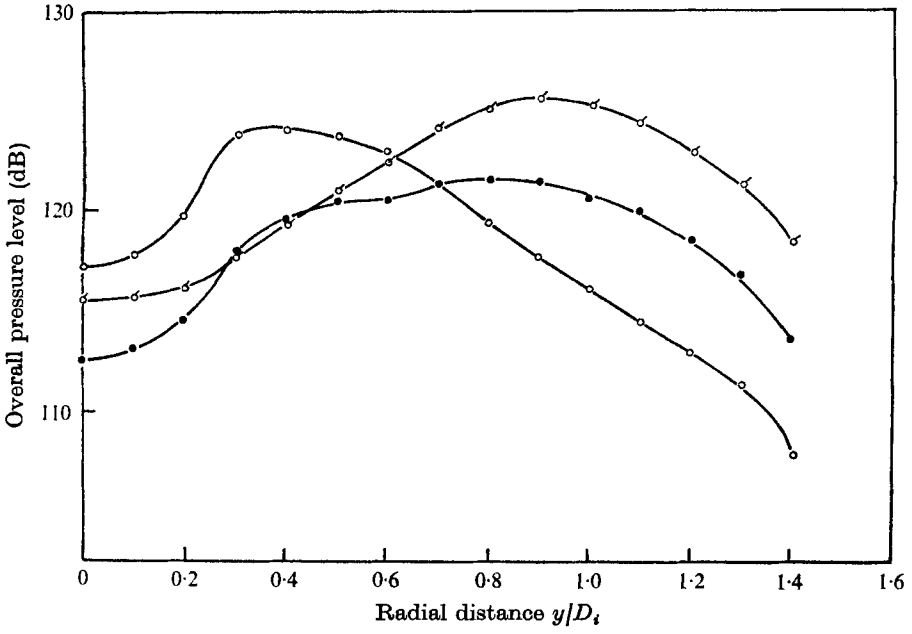

FIGURE 10. Radial distribution of overall pressure level in intermediate zone. $x/D_i = 3$. Symbols same as figure 9.

present investigation, Williams *et al.* (1969) observed in the far field an attenuation from the single-jet results in 3 dB at $\lambda = 0{\cdot}3$, 4 dB at $\lambda = 0{\cdot}5$ and 1 dB at $\lambda = 0{\cdot}7$. This attenuation is far less than the corresponding values 7, 12 and 14 dB of figure 9. Similarly, the peak further away from the coaxial-jet axis, the secondary peak, is found inside the secondary mixing region (figure 1). The location is again nearer to the boundary of the secondary potential core.

For the secondary peak, the maximum pressure level has opposite trends to the results of the primary peak. This means that, with the increase in the mean-velocity ratio λ, the maximum level increases from 119 dB at $\lambda = 0{\cdot}3$ to 124 dB at $\lambda = 0{\cdot}5$ and 126 dB at $\lambda = 0{\cdot}7$.

Looking at the radial distribution as a whole, the dominance of either the primary or secondary peaks depends on the mean-velocity ratio. With the introduction of the secondary jet with $\lambda = 0{\cdot}3$ the primary peak is more dominant. However, the level of the secondary peak is still fairly substantial, only about 4 dB less than the primary one.

With the increase in the secondary jet velocity, $\lambda = 0{\cdot}5$ and $0{\cdot}7$, the primary peak loses its dominance and is progressively replaced by the secondary. This loss in dominance of the primary peak, and the gain in that of the secondary, with the increase in mean-velocity ratio, can be explained by the reduction in shear in the primary mixing region and the increase in shear in the secondary mixing region.

In the intermediate zone $x/D_i = 3$, disregarding the two indistinct peaks at $\lambda = 0{\cdot}5$, basically one peak is found (figure 10). At $\lambda = 0{\cdot}3$ the peak is due to that in the primary mixing region. The attenuation of this from the single-jet result

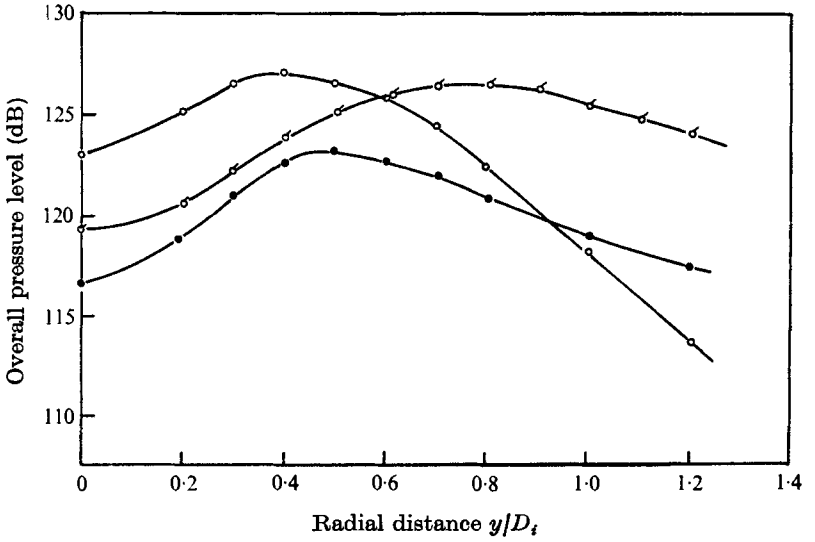

FIGURE 11. Radial distribution of overall pressure level in fully-merged zone. $x/D_i = 6$. Symbols same as figure 9.

amounts to 8 dB. At $\lambda = 0{\cdot}5$ this primary peak reduces in level, and becomes indistinct. Further increase in λ results in the complete disappearance of the primary peak. The secondary peak starts to increase in level from $\lambda = 0{\cdot}5$, and becomes dominant at $\lambda = 0{\cdot}7$.

From figure 10 it seems that one of the two peaks observed in the initial merging zone undergoes changes in the intermediate zone. At low mean-velocity ratios, the secondary peak disappears, while at high velocity ratios the primary peak disappears. This suggests preference for growth of vortices for a certain mode of disturbance, as suggested by Crow & Champagne (1971) and Chan (1974). Further discussion of this will be presented later.

In the fully-merged zone $x/D_i = 6$, the radial distributions of the overall pressure level show only one peak (figure 11). For low velocity ratios $\lambda = 0{\cdot}3$ and $0{\cdot}5$, it seems the primary peak is responsible, and it is found near the boundary of the primary potential cone. At $\lambda = 0{\cdot}7$, however, it seems the secondary peak is responsible. At this mean-velocity ratio, the location of the maximum is not near the potential cone boundary but at $y/D_i = 0{\cdot}8$. Comparison of the two lower velocity ratios shows the reduction in level with the increase in secondary velocity. At $\lambda = 0{\cdot}7$, the pressure level is about the same as the one at $\lambda = 0{\cdot}3$.

The pressure and correlation measurements inside the mixing region of a single jet by Fuchs (1972) and Lau *et al.* (1972) suggest that the peak in the overall pressure profile is due to the vortices or coherent structures inside the jet. Covariance measurements of Ko (1974) and Ko & Davies (1975) also suggest that the position of the maximum pressure level is where the vortices convect downstream.

Thus, from the pressure results shown in figures 9–11, two types of vortices are found in the two mixing regions inside the initial merging zone. The primary vortices are found in the mixing region of the primary jet; the secondary are

found in the mixing region of the secondary jet. As the vortices convect into the intermediate zone, decay or continuous growth of the vortices, either primary or secondary, would depend on the mean-velocity ratio. As will be shown later, continuous growth would depend on those that have the same Strouhal number as the preferred mode of disturbance. In this way, the decayed vortices would be absent in the fully-merged zone, leaving those that are preferred.

6. Spectrum inside coaxial jets

Spectra within the initial region of coaxial jets have been obtained with both a hot wire and a microphone. Since the pressure spectra obtained are basically the same as the velocity spectra, and since the velocity spectra are more illustrative, either type will be used for discussion.

The axial distributions of the velocity spectra along the axis of the coaxial jet $y/D_i = 0$, for the three different velocity ratios, are shown in figures 12–14. Instead of one single broad peak, as observed in single-jet results of Ko & Davies (1971), two peaks are found. Generally, as shown by the figures, one occurs at the low frequency of around 500 Hz, the other at the higher frequency of 1·8 kHz. The exact frequency of the peaks depends on the mean-velocity ratio, the axial and radial positions. The variation of these peak frequencies will be discussed in § 7, on the Strouhal number. The complete absence of a peak within the first half diameter also agrees with the single-jet results of Ko & Davies (1971). This means that the vortices are usually found at least half a diameter downstream.

For $\lambda = 0{\cdot}3$, the high-frequency peak starts to appear from $x/D_i = 0{\cdot}5$ (figure 12). At $x/D_i = 1$, the peak level builds up very rapidly for the next one and a half diameters. Then the rate of increase is reduced. However, there is still a continuous build-up of the peak level. The area under the high-frequency peak also increases. In other words, the frequency bandwidth under the broad peak increases with increase in axial distance. The same phenomenon was again observed in the single-jet measurements of Ko & Davies (1971).

This similarity of the coaxial-jet results with this mean-velocity ratio to the single-jet results is due to the low velocity ratio. At this value of $\lambda = 0{\cdot}3$, the mean-velocity difference between the primary and secondary jets is only slightly smaller than for a single jet in ambient air. This means that the primary mixing region at this velocity ratio is not greatly different from the mixing region of single jet. Further, this similarity leads to the conclusion that the vortices generated in the primary mixing region are responsible for the high-frequency peak.

It has been suggested by Lau *et al.* (1972) that the peak frequency observed is a function of the convection velocity of the vortices. Thus, it can be easily concluded that the high-frequency vortices are situated in the primary mixing region, where the local mean velocity, and thus the convection velocity, is high. On the other hand, the small mean-velocity difference between the secondary jet and the stationary ambient air and the low convection velocity of the vortices would be responsible for the low-frequency peak in the spectrum.

The presence of the secondary peak in the spectrum obtained at the jet axis

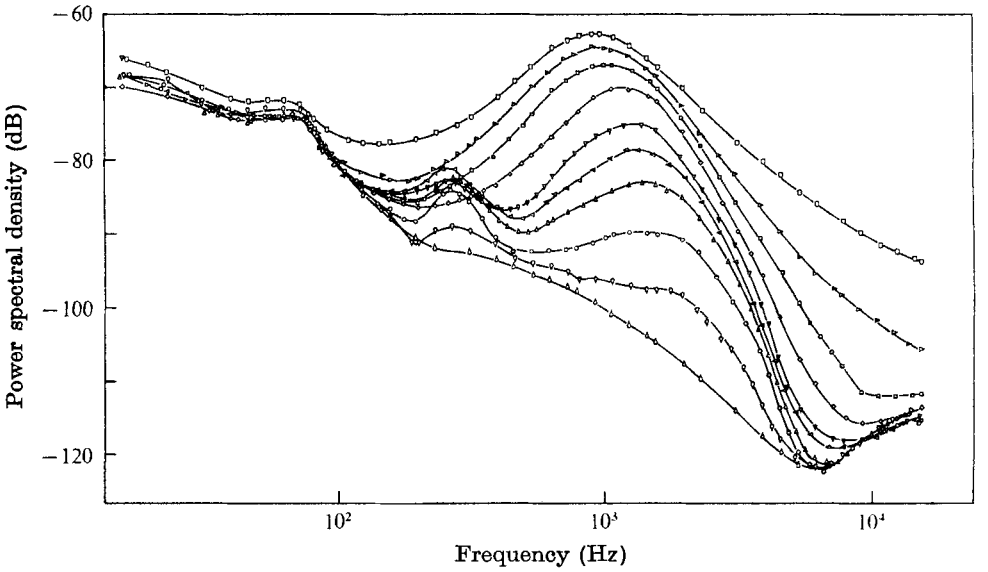

FIGURE 12. Power spectra for different axial positions at jet axis. $y/D_i = 0$. $\lambda = 0{\cdot}3$. Symbols same as figure 2.

means that the secondary vortices, though further away than the primary, still induce a field on the axis of the coaxial jets. The reason may be that there is no masking, owing to the low level of both the primary vortices and the background at the frequency range of the secondary peak.

The maximum level of the low-frequency or secondary peak shows an interesting phenomenon. Starting from $x/D_i = 0{\cdot}5$, it starts to increase, and it reaches its highest level at $x/D_i = 2{\cdot}5$. After $x/D_i = 2{\cdot}5$, it decreases, and disappears from the spectrum at $x/D_i = 4$. From the above results, the low-frequency peak, which is due to the vortices generated within the secondary mixing region, undergoes generation and decay within the first four primary diameters downstream from the nozzle exits. The vortices reach their maximum level at $x/D_i = 2{\cdot}5$ and decay very rapidly within the next one and a half primary diameters.

Furthermore, the axial position $x/D_i = 4$, where the vortices disappear, is within the intermediate zone. It is in this zone that both the primary, or high-frequency, and the secondary, or low-frequency, vortices convect and mix. Also, from the continuous increase in the high-frequency vortices over all the axial positions investigated, $x/D_i = 7$, and the rapid decay of the low-frequency vortices, the former vortices are not only dominant but also preferred (Crow & Champagne 1971; Chan 1974).

With the increase in the secondary velocity to $\lambda = 0{\cdot}5$, the maximum level of the high-frequency peak decreases (figure 13). However, with reduction in level, the maximum level still behaves like that of the lower mean-velocity ratio and increases continuously with axial distance downstream. This means that the primary vortices are still growing within the first seven primary diameters. The low-frequency peak, on the other hand, has a higher peak level than that at

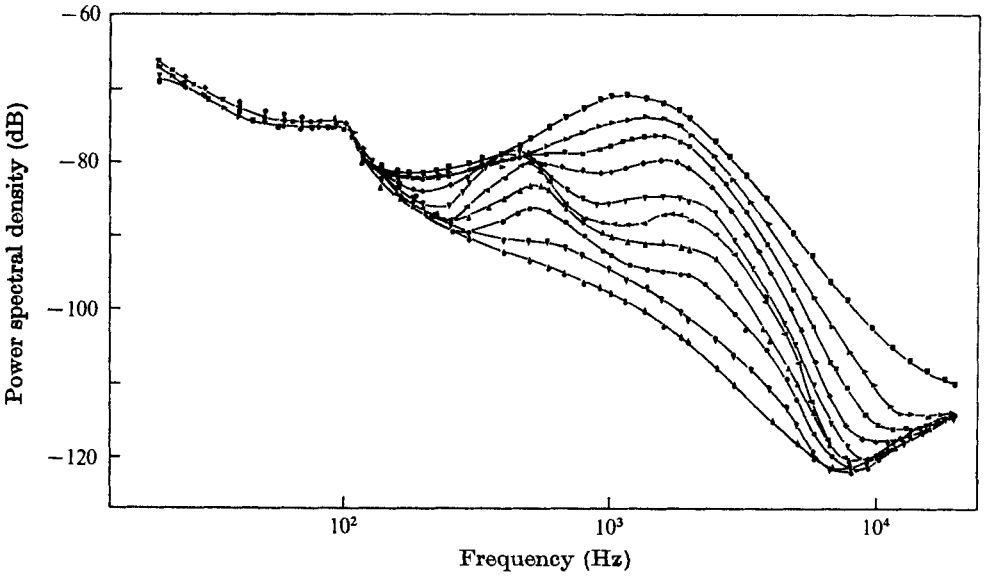

FIGURE 13. Power spectra for different axial positions at jet axis. $y/Di = 0$. $\lambda = 0{\cdot}5$. Symbols same as figure 2.

$\lambda = 0{\cdot}3$. The maximum level reaches its highest at an axial distance of x/D_i between 3 and 3·5. Further downstream, from $x/D_i = 5$ the peak either loses its significance, or is masked by the low-frequency components of the high-frequency vortices. Compared with the results for $\lambda = 0{\cdot}3$, the axial distances where the low-frequency vortices reach their highest value and disappear are found one diameter further downstream for this velocity ratio of $\lambda = 0{\cdot}5$. This means that slightly longer distances are required for the development of the vortices. But the same distance is necessary for the decay.

A different picture is shown in figure 14 for the spectra of the highest mean-velocity ratio $\lambda = 0{\cdot}7$. Both the low- and high-frequency peaks continue to grow over the axial distance investigated. Unlike the two lower velocity ratios, the low-frequency peak is dominant and the high-frequency peak is more or less insignificant.

The spectral results of the last three figures show that the variation of the peak levels of the two peaks agree well with the results of the overall pressure level. This implies that the energy under the peaks is responsible for the overall pressure shown in figures 9–11. This also indicates the dominance of either the high- or the low-frequency vortices that exist in the primary and secondary mixing regions. The background turbulence level is not significant. The above discussion of the peak level can be better illustrated by figure 15, in which the pressure and turbulence intensities of the peaks considered are included.

The pressure and velocity fluctuations presented in figure 15 are the estimated energies contained under the peaks in the spectra. Thus, the effect of local turbulence, if any, is excluded from the consideration. Further, the definitions of $\overline{U}_*$ and D_* adopted for the different jets are shown in table 1. Similar results are shown by both the pressure and the turbulence intensities (figure 15). For the

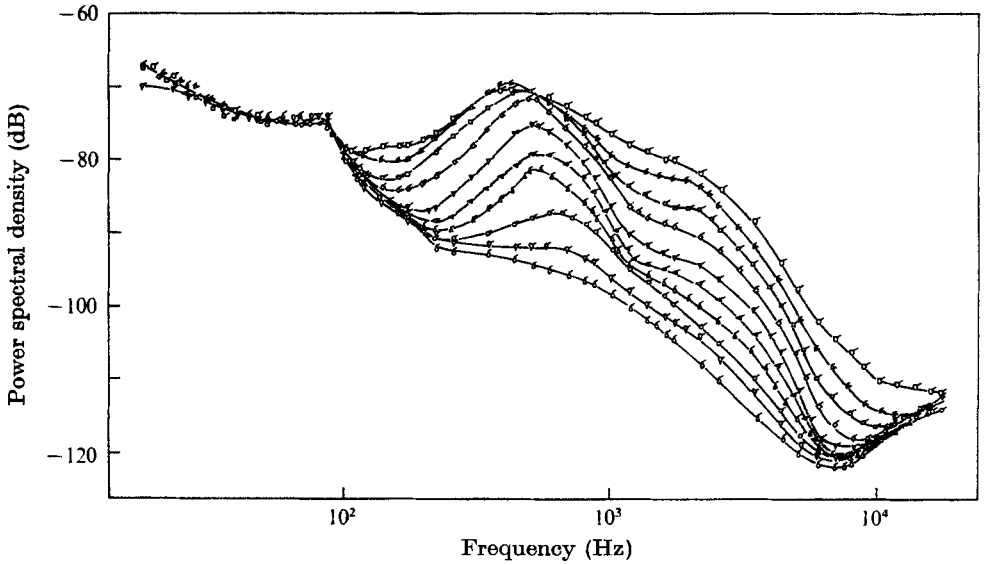

FIGURE 14. Power spectra for different axial positions at jet axis. $y/D_i = 0$, $\lambda = 0{\cdot}7$. Symbols same as figure 2.

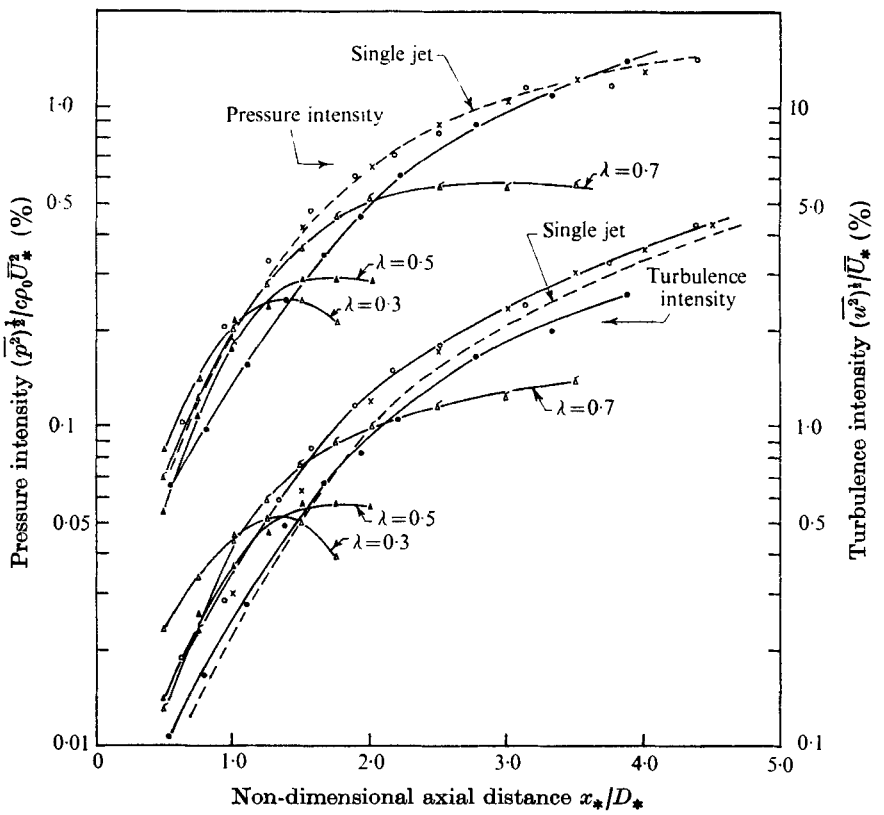

FIGURE 15. Turbulence and pressure intensities at jet axis. $y/D_i = 0$. Primary vortices. λ: ○, 0·3; ●, 0·5. Secondary vortices. λ: △, 0·3; ▲, 0·5; ⧊, 0·7. Single jet. ×, Fuchs (1972).

	Initial merging zone		Fully-merged zone		Single jet
	Primary vortices	Secondary vortices			
Mean velocity ratio λ	0·3, 0·5, 0·7	0·3, 0·5, 0·7	0·3, 0·5, 0·7		0
Diameter D_*	D_i	D_0	$D_e = (1+\lambda^2\beta)^{\frac{1}{2}} D_i$		D
Exit velocity $\overline{U}_*$	$\overline{U}_i - \overline{U}_0$	$\overline{U}_0$	$\overline{U}_e = \overline{U}_i$		$\overline{U}_{\text{exit}}$
Axial distance x_*	$x/\Delta L$	x	$x - \Delta x$		x
Non-dimensional axial distance x_*/D_*	$\dfrac{x}{\Delta L D_i}$	$\dfrac{x}{D_0}$	$\dfrac{x-\Delta x}{D_e}$		$\dfrac{x}{D}$
Non-dimensional radial distance y/D_*	$\dfrac{y-y_{0.5}}{y_{0.9}-y_{0.1}}$	$\dfrac{y}{D_0}$	$\dfrac{y}{D_e}$		$\dfrac{y}{D}$
Non-dimensional radial distance η_*	$\eta_i = \dfrac{y-\frac{1}{2}D_i}{x/\Delta L}$	$\eta_0 = \dfrac{y-\frac{1}{2}D_0}{x}$	$\eta_e = \dfrac{y-\frac{1}{2}D_e}{x-\Delta x}$		$\eta = \dfrac{y-\frac{1}{2}D}{x}$
Mean velocity ratio λ			0·3, 0·5	0·7	
Turbulence intensity $(\overline{u}^2)^{\frac{1}{2}}/\overline{U}_*$	$\dfrac{(\overline{u}^2)^{\frac{1}{2}}}{\overline{U}_i - \overline{U}_0}$	$\dfrac{(\overline{u}^2)^{\frac{1}{2}}}{\overline{U}_0}$	$\dfrac{(\overline{u}^2)^{\frac{1}{2}}}{\overline{U}_i}$	$\dfrac{(\overline{u}^2)^{\frac{1}{2}}}{\overline{U}_0}$	$\dfrac{(\overline{u}^2)^{\frac{1}{2}}}{\overline{U}_{\text{exit}}}$
Pressure intensity $\dfrac{(\overline{p}^2)^{\frac{1}{2}}}{c\rho_0 \overline{U}_*^2}$	$\dfrac{(\overline{p}^2)^{\frac{1}{2}}}{c\rho_0(\overline{U}_i - \overline{U}_0)^2}$	$\dfrac{(\overline{p}^2)^{\frac{1}{2}}}{c\rho_0 \overline{U}_0^2}$	$\dfrac{(\overline{p}^2)^{\frac{1}{2}}}{c\rho_0 \overline{U}_i^2}$	$\dfrac{(\overline{p}^2)^{\frac{1}{2}}}{c\rho_0 \overline{U}_0^2}$	$\dfrac{(\overline{p}^2)^{\frac{1}{2}}}{c\rho_0 \overline{U}_{\text{exit}}^2}$
Strouhal number St_*	$\dfrac{f_p D_i}{[0{\cdot}6(\overline{U}_i - \overline{U}_0) + \overline{U}_0]/0{\cdot}6}$	$\dfrac{f_p D_0}{\overline{U}_0}$	$\dfrac{f_p D_e}{\overline{U}_i}$	$\dfrac{f_p D_0}{\overline{U}_0}$	$\dfrac{f_p D}{\overline{U}_{\text{exit}}}$

TABLE 1. Summary of different definitions of coaxial jets. Note: ΔL = (length of primary potential core with secondary flow)/(length of primary potential core with no secondary flow).

high-frequency vortices, which exist in the primary mixing region of coaxial jets with $\lambda = 0{\cdot}3$ and 0·5, the intensities agree very well with the single-jet results of Fuchs (1972). This means that continuous growth of both intensities, and thus vortices, is observed within the first five diameters downstream x/D_*. This good agreement suggests that the high-frequency vortices have the same characteristics as the vortices of the single jet.

Initially, the low-frequency vortices have the same growth rate as the high-frequency. For $\lambda = 0{\cdot}3$ the vortices start to decay from an axial distance of $x/D_* = 1{\cdot}5$. With increase in λ, the maximum intensities increase, and the axial position at which decay starts progressively shifts further downstream: $x/D_* = 1{\cdot}8$ for $\lambda = 0{\cdot}5$ and $x/D_* = 2{\cdot}5$ for $\lambda = 0{\cdot}7$. The latter case tends to approach the characteristics of high-frequency vortices and of single jets (Ko & Davies 1975). That these characteristics of the low-frequency vortices at $\lambda = 0{\cdot}7$ are similar to those of a single jet seems logical. As has been discussed, it is due to the fact that the mean-velocity difference between the secondary jet and the stationary ambient air approaches that of the single jet.

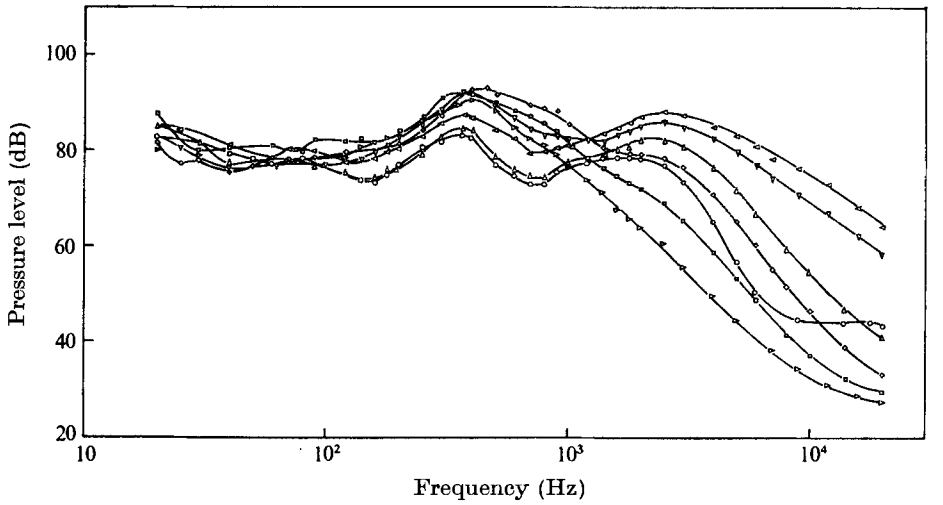

FIGURE 16. Pressure spectra for different radial positions in initial merging zone. $x/D_i = 2$ $\lambda = 0{\cdot}3$. y/D_i: ○, 0; △, 0·2; ◁, 0·4; ▽, 0·6; ◇, 0·8; □, 1·0; ▷, 1·2.

The different rate of decay of the low-frequency vortices at different λ shown in figure 15 is interesting. At $\lambda = 0{\cdot}3$ the vortices experience the highest rate of decay; thus the shortest distance for which the peak is detected in the spectra (figure 12). However, it may still be present but masked by the higher energy level of the high-frequency peak. At $\lambda = 0{\cdot}5$, the rate of decay is much slower, and it is further downstream that the low-frequency peak is masked.

The radial distribution of the velocity spectrum inside the coaxial jets is not shown. It is due to the masking of peaks by the strong local turbulence in the two mixing regions, observed by Ko & Davies (1971). In this respect, it is more beneficial to look at the pressure spectra in which the masking effect is more or less absent.

Figures 16–18 show the radial distribution of the pressure spectra within the initial merging zone $x/D_i = 2$. At $\lambda = 0{\cdot}3$, the inner potential core has two peaks (figure 16). As the inner mixing region is approached, the high-frequency peak increases in level, and reaches its maximum at about $y/D_i = 0{\cdot}4$. This radial position is just within the inner mixing region. With further increase in radial distance $y/D_i \geqslant 0{\cdot}6$, figure 16 gives rapid reduction in the peak level of high-frequency vortices. At $y/D_i = 0{\cdot}9$, the peak more or less disappears. The low-frequency peak, however, is found over the whole radial distance considered. Its peak level increases from the axis, and reaches its maximum at about $y/D_i = 0{\cdot}9$.

At $\lambda = 0{\cdot}5$, the high-frequency peak decreases when compared with that obtained at $\lambda = 0{\cdot}3$. The low-frequency peak, however, increases (figure 17). As in the case of $\lambda = 0{\cdot}3$, the low-frequency peak is observed over the whole radial distance considered. However, the high-frequency peak is observed only for $y/D_i \leqslant 0{\cdot}6$. The approximate location of the maximum peak level of the low-frequency peak is at $y/D_i = 0{\cdot}9$, and for the high-frequency is at $y/D_i = 0{\cdot}4$.

With further increase in the secondary velocity, $\lambda = 0{\cdot}7$, the high-frequency peak becomes even less dominant (figure 18). Similar to the results for the two

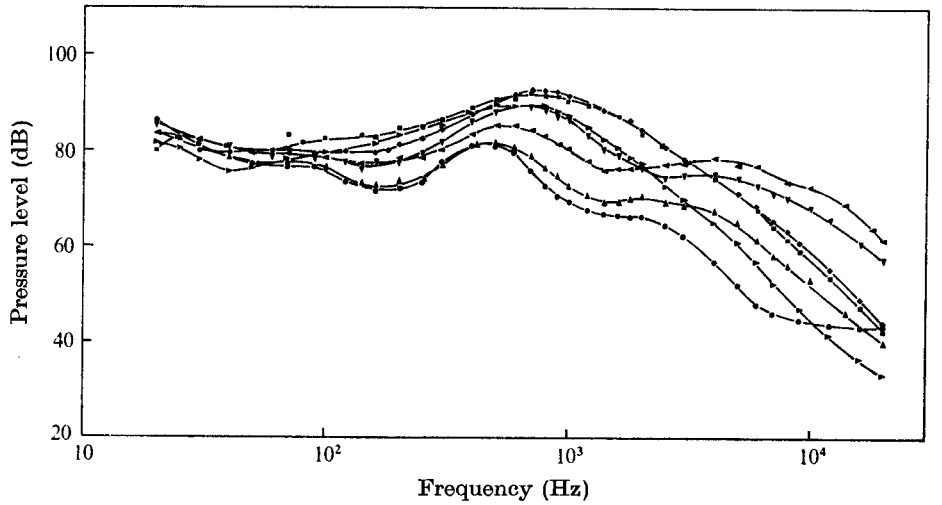

FIGURE 17. Pressure spectra for different radial positions in initial merging zone. $x/D_i = 2$, $\lambda = 0{\cdot}5$. y/D_i: ●, 0; ▲, 0·2; ◀, 0·4; ▼, 0·6; ◆, 0·8; ■, 1·0; ▶, 1·2.

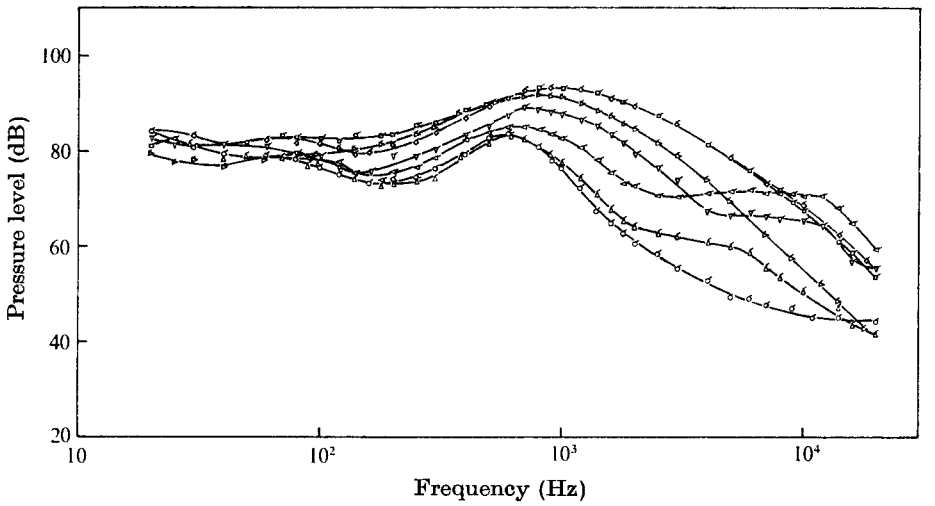

FIGURE 18. Pressure spectra for different radial positions in initial merging zone. $x/D_i = 2$, $\lambda = 0{\cdot}7$. y/D_i: ○, 0; △, 0·2; ◁, 0·4; ▽, 0·6; ◇, 0·8; □, 1·0; ▷, 1·2.

lower mean-velocity ratios, the low-frequency peak is found over the whole radial distance considered. The high-frequency peak is observed only for $y/D_i \leqslant 0{\cdot}8$. The corresponding estimated radial positions for the maximum of the low-frequency peak is at $y/D_i = 0{\cdot}9$, and for the high-frequency peak is at $y/D_i = 0{\cdot}4$.

From the above results within the initial merging zone, it is interesting to find that the low-frequency peak covers the whole radial position considered $0 \leqslant y/D_i \leqslant 1{\cdot}2$, while the high-frequency peak covers only the radial distance $y/D_i \leqslant 0{\cdot}9$. This absence of the high-frequency peak is particularly noticeable at $\lambda = 0{\cdot}3$. It might in part be due to the masking effect of the increased level at the frequency of the low-frequency peak. The other reason might be the absence

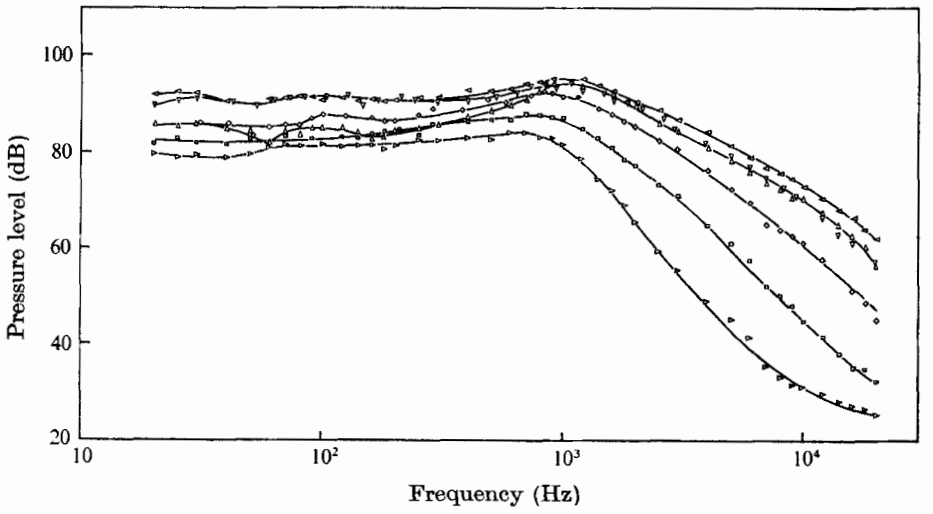

FIGURE 19. Pressure spectra for different radial positions in fully-merged zone. $x/D_i = 6$, $\lambda = 0{\cdot}3$. Symbols same as figure 16.

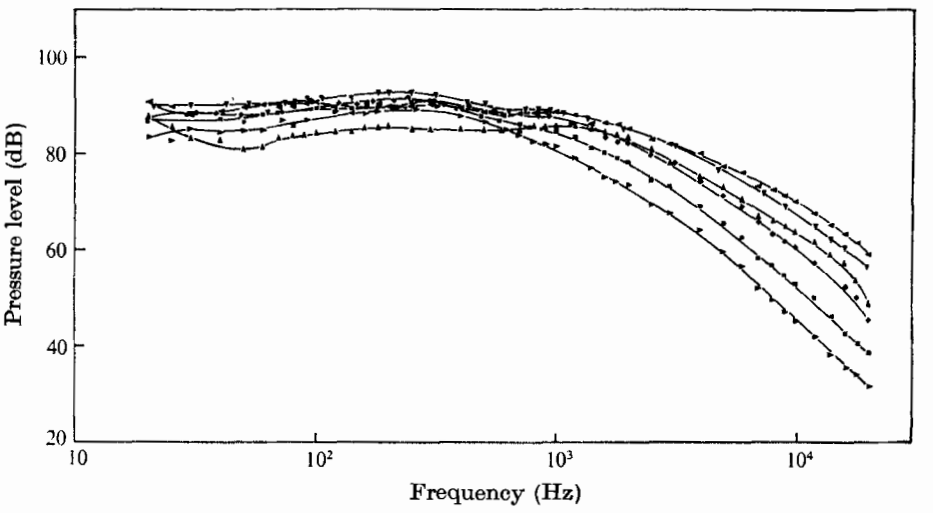

FIGURE 20. Pressure spectra for different radial positions in fully-merged zone. $x/D_i = 6$, $\lambda = 0{\cdot}5$. Symbols same as figure 17.

of the induced field of the high-frequency vortices in the secondary mixing region.

This absence of the induced field of the high-frequency vortices for $y/D_i \geqslant 0{\cdot}9$, and the presence of the low-frequency vortices over the whole radial distance, may indicate a difference in rate of development and size of the two types of vortices. The wider effect of the low-frequency vortices indicates that they are larger in size than the high-frequency. This is expected, since the low-frequency are generated in the outer mixing region, which has a larger scale (characteristic length) than the inner mixing region.

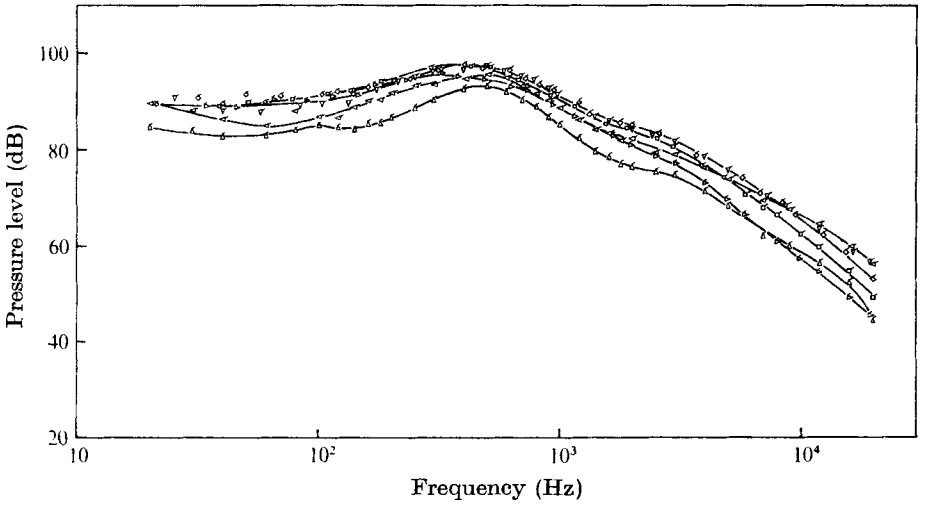

FIGURE 21. Pressure spectra for different radial positions in fully-merged zone. $x/D_i = 6$, $\lambda = 0{\cdot}7$. Symbols same as figure 18.

The radial distribution of the pressure spectra inside the fully-merged zone $x/D_i = 0{\cdot}6$ is shown in figures 19–21. The dominance of either the high-frequency or the low-frequency vortices depends on the mean-velocity ratio. At the velocity ratio $\lambda = 0{\cdot}3$, the peak shown in the spectra of figure 19 is similar to the high-frequency peak obtained at the axis (figure 12). This means that the high-frequency vortices are the dominant ones in this zone. Furthermore, the extent of the influence of these high-frequency vortices covers the whole radial distance considered $y/D_i \leqslant 1{\cdot}2$. This further supports the idea of the continuous growth of these vortices suggested above.

At the same velocity ratio $\lambda = 0{\cdot}3$, the disappearance of the low-frequency peak over the whole radial distance considered agrees with the result discussed above (figures 19 and 12), that the low-frequency vortices have decayed in the intermediate zone. At the higher velocity ratio $\lambda = 0{\cdot}5$, the two peaks are only marginally above the background levels, and their presence depends on radial position. The high-frequency vortices can only be traced between $0{\cdot}2 \leqslant y/D_i \leqslant 0{\cdot}8$, and the low-frequency between $0{\cdot}4 \leqslant y/D_i \leqslant 1{\cdot}2$. The extent of the low-frequency vortices has been diminished (i.e. the effect of its influence is not felt at and near the jet axis $y/D_i \leqslant 0{\cdot}4$). This is different from the results in the initial merging zone (figure 17), where the effect of the low-frequency vortices is felt across the coaxial jet.

With further increase in the secondary jet velocity to $\lambda = 0{\cdot}7$, figure 21 shows the disappearance of the high-frequency vortices. In other words, the low-frequency vortices become dominant. The extent of their influence is over the whole radial distance considered.

Comparison of the spectra obtained in the two zones indicates that at the low velocity ratio $\lambda = 0{\cdot}3$, the higher-frequency vortices, which are generated in the primary mixing region, maintain their growth in the intermediate and fully-merged zones (figure 15). The low-frequency vortices, which are generated in the

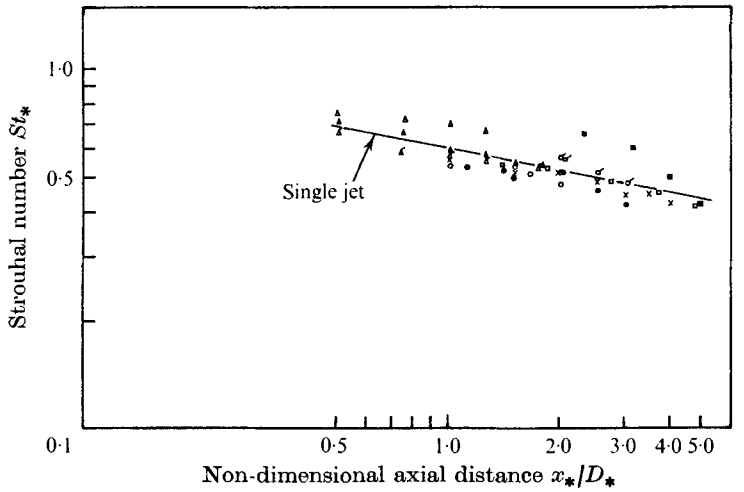

FIGURE 22. Strouhal number against axial distance at jet axis. $y/D_i = 0$. Initial merging zone. *Primary vortices*, λ: ○, 0·3; ●, 0·5; ◌́, 0·7. *Secondary vortices*. λ: △, 0·3; ▲, 0·5; ◭, 0·7. Fully-merged zone. λ: □, 0·3; ■, 0·5; □́, 0·7. Single jet. ×, Ko & Davies (1971).

secondary mixing region, start to decay in the intermediate zone. They become insignificant even before reaching the fully-merged zone. At $\lambda = 0{\cdot}5$ both types of vortices convect downstream, and can still be observed in the fully-merged zone. It seems there is little decay over the axial distance considered. At $\lambda = 0{\cdot}7$ the opposite trend from that of $\lambda = 0{\cdot}3$ is found. The low-frequency vortices are dominant in the initial merging zone. Even in the fully-merged zone, they still maintain their dominance. On the other hand, the high-frequency vortices undergo decay.

Thus, the above discussion shows what happens when the two types of vortices, generated in the primary and secondary mixing regions, mix in the intermediate zone. It is here that either one or both types of vortices are preferred for continuous growth and convection downstream.

7. Strouhal number

As shown by the spectra obtained at the jet axis (figures 12–14), the peak frequency of the two types of vortices varies with the mean-velocity ratio and axial position. With increase in mean-velocity ratio, the peak frequency of the two vortices also increases. However, with increase in axial distance, the peak frequency of both peaks decreases, like the single-jet results of Ko & Davies (1971).

The peak frequency is expressed in the form of a Strouhal number $St_* = f_p D_*/\overline{U}_*$. Because of the complicated structures within the coaxial jets, different forms of Strouhal number are used for different zones and velocity ratios (table 1). The calculated Strouhal numbers of different sources and in different zones are shown in figure 22. The corresponding Strouhal numbers of the single jet, as obtained by Ko & Davies (1971), are also shown. Figure 22 exhibits very good agreement of the results for different coaxial jets with the single jet. The results show a gradual

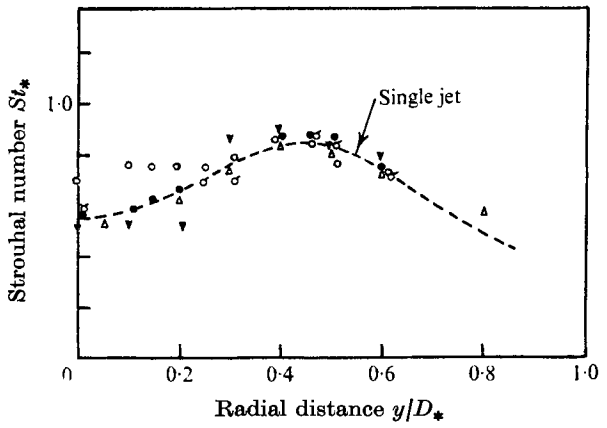

FIGURE 23. Strouhal number against radial distance in initial merging zone. $x/D_* = 1{\cdot}0$. λ: ○, 0·3; ●, 0·5; ♂, 0·7. $x/D_* = 1{\cdot}25$. λ: △, 0·3; ▼, 0·5. Single jet, $x/D = 1$: ———, Lau *et al.* (1972).

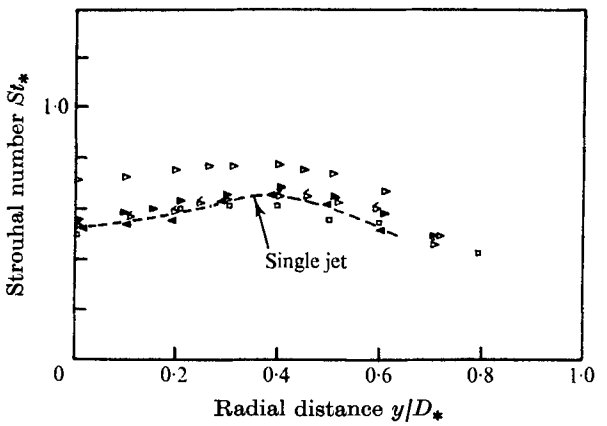

FIGURE 24. Strouhal number against radial distance in intermediate zone. $x/D_* = 1{\cdot}5$. λ: ▷, 0·3; ▶, 0·5; ⊳, 0·7. $x/D_* = 1{\cdot}9$. λ: □, 0·3; ◀, 0·5. Single jet, $x/D = 1{\cdot}5$: ———, Ko & Davies (1971).

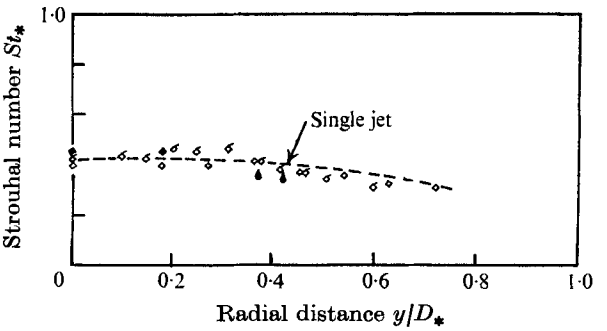

FIGURE 25. Strouhal number against radial distance in fully-merged zone. $x/D_i = 6$. λ: ◇, 0·3; ◆, 0·5. Primary vortices. ♦, $\lambda = 0{\cdot}5$. Secondary vortices. ◇, $\lambda = 0{\cdot}7$. Single jet, $x/D = 3$: ———, Ko & Davies (1971).

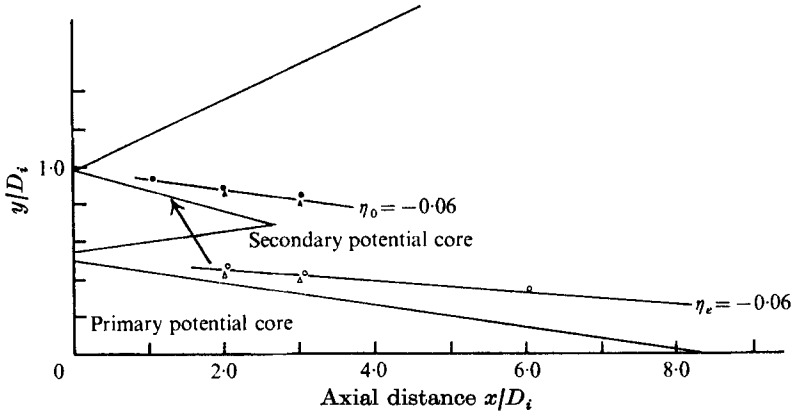

FIGURE 26. Profile of initial region of coaxial jet. $\lambda = 0{\cdot}5$. Overall pressure: ○, primary vortices; ●, secondary vortices. Strouhal number: △, primary vortices; ▲, secondary vortices.

decrease in the Strouhal number with axial distance. Near the end of the potential core $x_*/D_* = 5$, the Strouhal number is about 0·5.

Similarly, the radial distribution of the Strouhal number of the peak frequency of the two types of vortices is shown in figures 23–25. Results of Ko & Davies (1971) and Lau *et al.* (1972) are also shown. Agreement between the Strouhal number of the two types of vortices within the primary and secondary mixing regions and with the vortices of the single jet is extremely good. Somewhat as in the case of the single-jet measurements, a maximum Strouhal number is found for the axial positions $x_*/D_* = 1$ and 1·5, but no peak is found for $x_*/D_* = 3$. The radial positions of the maximum Strouhal number are situated at $y/D_* = 0{\cdot}45$ for $x_*/D_* = 1{\cdot}0$ and $y/D_* = 0{\cdot}4$ for $x_*/D_* = 1{\cdot}5$. These locations are near the inner boundary of the mixing region with the potential cone (figure 26).

The location of the maximum Strouhal number is the same as the location of maximum pressure. They both fall on the radial position $\eta_* = -0{\cdot}06$, where the vortices are convecting downstream (Ko 1974; Ko & Davies 1975).

Crow & Champagne (1971) and Chan (1974) found that the preferred or most amplified mode in the single jet has a Strouhal number of between 0·3 and 0·35. Artificial excitation can describe the preferred mode of excitation within the jet fairly accurately. However, in the case of the single jet, the Strouhal number measured at the axis is roughly between 0·5 and 0·6. This is different from the preferred mode obtained by artificial excitation. This difference means that, although the most preferred mode is between 0·3 and 0·35, the jet itself (without any artificial excitation) may be excited by disturbances that have the same Strouhal number of 0·5. The sources of these disturbances seem to be derived from the tiny turbulence at the nozzle exit, usually less than 1 %. This argument is supported by the results of Crow & Champagne (1971) that at very low levels, less than 0·05, the mode having the higher Strouhal number of about 0·5 is more preferred than that at 0.3. This explanation is reasonable, because of the very small turbulence level at the nozzle exit, and because the energy of the turbulence at frequencies having a Strouhal number of about 0·5 is smaller still. This is

further supported by the position of the maximum excited amplitude of the mode with Strouhal number 0·5. Chan (1974) found that at this Strouhal number the position is near $x/D = 2{\cdot}5$. This is in exact agreement with the maximum covariance level obtained by Ko (1974) and Ko & Davies (1975).

After initial merging in the initial merging zone, the turbulence field undergoes transition in the intermediate zone, where mixing of the fluid issued from the upstream mixing regions occurs, resulting in an equivalent jet of diameter D_e. Therefore, in the intermediate zone, the Strouhal number $f_p D_e/\bar{U}_i$ of the preferred mode is about 0·5.

In the intermediate zone and at $\lambda = 0{\cdot}3$, the Strouhal number of the secondary vortices is about 0·13, and that of the primary vortices is about 0·5. The Strouhal number of the primary vortices, with a value of 0·5, is closer to the preferred value. Thus, it is not surprising that the primary vortices maintain their growth within the intermediate and fully-merged zones (figure 15). The Strouhal number of the secondary vortices, 0·13, differs vastly from the preferred, and they decay inside the intermediate zone. Similarly, for $\lambda = 0{\cdot}5$, the Strouhal numbers of the primary and secondary vortices at the axial position where the intermediate zone begins are about 0·6 and 0·2. Using the same criterion, the primary vortices are still preferred to the secondary (figure 15). For $\lambda = 0{\cdot}7$, the Strouhal number of the primary and secondary vortices is about 1·3 and 0·35. Thus, the secondary vortices are preferred and grow further in the intermediate zone. The rate of growth has decreased when compared with the most amplified mode having a Strouhal number of about 0·5 (figure 15).

8. Conclusions

The mean-velocity measurements within the initial region of coaxial jets isolate three separate zones: the initial merging, the intermediate and the fully-merged zone. In the initial merging and fully-merged zones, similarity of the mean-velocity profiles in the three mixing regions has been obtained. The similarity agrees very well with the single-jet results. In the intermediate zone, no similarity is obtained.

Similarity of the turbulence-intensity profiles of the three mixing regions, inside the initial merging and fully-merged zones, is also obtained. It used the same non-dimensional radial distances as were used for the mean-velocity profiles. Fairly good agreement with the single-jet results is again found.

Overall pressure measurements within coaxial jets show two different peaks due to the vortices generated in the primary and secondary mixing regions. Combined with the detailed spectral results, these demonstrate that the high-frequency vortices are generated in the primary mixing region, where the convection velocity is high. The low-frequency vortices, however, are generated in the secondary mixing region, where the convection velocity is low. From the similarity and spectral measurements, there is evidence that the primary vortices are generated further upstream than the secondary. The difference can be between a half and one primary diameter.

The merging of the two mixing regions in the intermediate zone involves com-

plicated mixing of the two types of vortices. Further growth or decay of either the primary or secondary vortices further downstream seems to depend on Strouhal number. Vortices having a Strouhal number between 0·3 and 0·5 would experience continuous growth even in the fully-merged zone. Any other Strouhal number would see rapid decay of the vortices.

The dominance of either type of vortices, or both, depends on the mean-velocity ratio. At a low mean-velocity ratio $\lambda = 0{\cdot}3$, the high-frequency vortices are more dominant. At $\lambda = 0{\cdot}5$, the high-frequency are still dominant, but the dominance of the low-frequency is increasing. At a high mean-velocity ratio $\lambda = 0{\cdot}7$, the low-frequency vortices become the only dominant ones.

The Strouhal number of the peak frequency of the vortices within the three mixing regions agrees very well with the single-jet results. The peak of the Strouhal number is found in the radial distribution. It is at the same $\eta_* = -0{\cdot}06$.

The good agreement of the results of coaxial and single jets suggests a simplified approach to understand the complicated flow structure of coaxial jets. This can be considered simply as a combination of several single jets with characteristics the same as those of a single jet discharging into stationary ambient air.

REFERENCES

Abramovich, N. 1963 *The Theory of Turbulent Jets.* M.I.T. Press.

Bradshaw, P., Ferriss, D. H. & Johnson, R. F. 1964 Turbulence in the noise-producing region of a circular jet. *J. Fluid Mech.* **19**, 591–624.

Chan, Y. Y. 1974 Spatial wave in turbulent jets. *Phys. Fluids*, **17**, 46–53.

Chigier, N. A. & Beer, J. M. 1964 The flow region near the nozzle in double concentric jets. *Trans. A.S.M.E., J. Basic Engng*, **86**, 797–804.

Crow, S. C. & Champagne, F. H. 1971 Orderly structure in jet turbulence. *J. Fluid Mech.* **48**, 547–591.

Davies, P. O. A. L. & Davis, M. R. 1966 Hot-wire anemometer. *I.S.A.V. Rep.* no. 155.

Davies, P. O. A. L., Fisher, M. J. & Barratt, M. J. 1963 The characteristics of the turbulence in the mixing region of a round jet. *J. Fluid Mech.* **15**, 337–367.

Eldred, K. M. *et al.* 1971 Far-field noise generation by coaxial flow jet exhaust. 1. Detailed discussion. *Wyle Lab. Rep. FAA-RD*-71-101, 1.

Forstall, W. &. Shapiro, H. H. 1950 Momentum and mass transfer in coaxial gas jets. *Trans. A.S.M.E., J. App. Mech.* **10**, 399–408.

Fuchs, H. V. 1972*a* Measurement of pressure fluctuations within subsonic turbulent jets. *J. Sound Vib.* **22**, 361–378.

Fuchs, H. V. 1972*b* Space correlations of the fluctuating pressure in subsonic turbulent jets. *J. Sound Vib.* **23**, 77–99.

Gelb, G. H. & Martin, W. A. 1966 An experimental investigation of the flow field about a subsonic jet exhausting into a quiescent and a low velocity air stream. *Can. Aero. Space J.* **12**, 333–342.

Ko, N. W. M. 1974 On the correlation technique in the subsonic jet. *Noise, Shock Vibration Conf.* Monash University, Melbourne, pp. 226–235.

Ko, N. W. M. & Davies, P. O. A. L. 1971 The near field within the potential cone of subsonic cold jets. *J. Fluid Mech.* **50**, 49–78.

Ko, N. W. M. & Davies, P. O. A. L. 1975 Some covariance measurements in a subsonic jet. *J. Sound Vib.* **41**, 347–358.

Ko, N. W. M. & Kwan, A. S. H. 1974 Experimental investigation of subsonic coaxial jets. *5th Australian Conf. on Hydraulics and Fluid Mech.*, Canterbury University Christchurch, pp. 609–616.

LAU, J. C., FISHER, M. J. & FUCHS, H. V. 1972 The intrinsic structure of turbulent jets. *J. Sound Vib.* **22**, 379–406.

LAUFER, J. 1974 On the mechanism of noise generation by turbulence. *University of Southern California, Los Angeles, USCAE* 125.

MOLLO-CHRISTENSEN, E., KOLPIN, M. A. & MARTUCCELLI, J. R. 1964 Experiments on jet flows and jet noise for field spectra and directivity patterns. *J. Fluid Mech.* **18**, 285–301.

NAKAMURA, A., MATSUMOTO, R., SUGIYAMA, A. & TANAKA, T. 1969 Some investigation on output level of microphone in airstream. *J. Acoust. Soc. Am.* **46**, 1391–1396.

WILLIAMS, T. J., ALI, M. R. M. H. & ANDERSON, J. S. 1969 Noise and flow characteristics of coaxial jets. *J. Mech. Engng Sci.* **11**, 133–142.